ESC European Society of Cardiology

Cardiovascular Research (2021) **117**, 533–546
doi:10.1093/cvr/cvaa016

# Hepatocyte growth factor-regulated tyrosine kinase substrate is essential for endothelial cell polarity and cerebrovascular stability

**Zhenyang Yu[1†], Jian Zeng[1†], Jun Wang [1], Yaxiong Cui[1], Xiaopeng Song[1], Yizhe Zhang[1], Xuan Cheng[1], Ning Hou[1], Yan Teng[1], Yu Lan[1], Yeguang Chen[2], and Xiao Yang [1*]**

[1]State Key Laboratory of Proteomics, Beijing Proteome Research Center, National Center for Protein Sciences (Beijing), Beijing Institute of Lifeomics, Beijing 102206, China; and[2]The State Key Laboratory of Biomembrane and Membrane Biotechnology, Tsinghua-Peking Center for Life Sciences, School of Life Sciences, Tsinghua University, Beijing 100084, China

*Received 3 June 2019; revised 5 November 2019; editorial decision 3 January 2020; accepted 31 January 2020; online publish-ahead-of-print 11 February 2020*

**Time for primary review: 30 days**

**Aims** Hepatocyte growth factor-regulated tyrosine kinase substrate (Hgs), a key component of the endosomal sorting complex required for transport (ESCRT), has been implicated in many essential biological processes. However, the physiological role of endogenous Hgs in the vascular system has not previously been explored. Here, we have generated brain endothelial cell (EC) specific *Hgs* knockout mice to uncover the function of Hgs in EC polarity and cerebrovascular stability.

**Methods and results** Knockout of *Hgs* in brain ECs led to impaired endothelial apicobasal polarity and brain vessel collapse in mice. We determined that Hgs is essential for recycling of vascular endothelial (VE)-cadherin to the plasma membrane, since loss of Hgs blocked trafficking of endocytosed VE-cadherin from early endosomes to recycling endosomes, and impaired the motility of recycling endosomes. Supportively, overexpression of the motor kinesin family member 13A (KIF13A) restored endosomal recycling and rescued abrogated polarized trafficking and distribution of VE-cadherin in Hgs knockdown ECs.

**Conclusion** These data uncover a novel physiological function of Hgs and support an essential role for the ESCRT machinery in the maintenance of EC polarity and cerebrovascular stability.

**Keywords** Hgs • VE-cadherin • Endothelial cell polarity • Cerebral vasculature • Endocytic recycling pathway

## 1. Introduction

Cerebral vasculature is predominantly composed of highly polarized brain endothelial cells (ECs), characterized by asymmetrical distribution of tight and adherens junctions, as well as various substrate-specific transporters.[1] Establishment of endothelial apicobasal polarity generates asymmetry along the apical–basal axis of ECs and is critical for the formation and maintenance of blood vessels.[2,3] However, how the apicobasal polarity of brain EC is maintained remains largely unknown.

The establishment and maintenance of apicobasal polarity of ECs involves a co-ordinated molecular network of cell–cell junctional complexes, cell–matrix junctions, polarity protein complexes, and cytoskeletal remodelling molecules.[4] Vascular endothelial (VE)-cadherin, the major cell adhesion protein at endothelial junctions, plays an essential role in the initiation of EC polarity.[5,6] VE-cadherin initiates EC apicobasal polarity by regulating the polarized distribution of CD34-sialomucins and cytoskeletal proteins such as CD34, podocalyxin (PODXL), Moesin, and F-actin at the apical membrane initiation site (AMIS).[5] VE-cadherin interacts with various polarity proteins and regulators to regulate endothelial apicobasal polarity and blood vessel lumen formation.[6–8] Deletion of *VE-cadherin* in both mice and zebrafish leads to impaired EC polarity and consequent aberrant lumen morphogenesis.[9–11] Polarized

* Corresponding author. Tel/fax: +86 10 63895937, E-mail: yangx@bmi.ac.cn

† The first two authors contributed equally to this article.

VE-cadherin dynamics has recently been demonstrated to be critical for angiogenesis,[12,13] suggesting that the dynamic distribution of endothelial VE-cadherin needs to be carefully restricted to maintain EC polarity.

Recent studies have revealed the emerging roles of endocytic recycling pathways in cell apicobasal polarization.[14] To maintain cell surface asymmetry, some endocytosed polarity proteins are recycled back to their polarized plasma membrane localization instead of being targeted for degradation.[15] Recycling occurs either directly, from Rab4-positive recycling endosomes to the plasma membrane (the fast recycling pathway), or indirectly, via Rab11-positive recycling endosomes (the slow recycling pathway).[16,17] The formation and recycling of tubular slow recycling endosomes can be facilitated by kinesin motor protein KIF13A.[17,18] The highly conserved endosomal sorting complex required for transport (ESCRT) machinery functions in endosomal sorting of ubiquitylated membrane proteins and generation of multivesicular bodies (MVBs).[19,20] Previous studies have revealed that the ESCRT machinery plays an essential role in polarization of epithelial cells and fibroblasts by regulating the intracellular trafficking of cell junctional molecules and cytoskeletal proteins.[21,22] Hepatocyte growth factor-regulated tyrosine kinase substrate (Hgs, also known as HRS) is a key component of ESCRT-0, which plays a critical role in initiating the ESCRT pathway through recognizing ubiquitylated cargo and recruiting the ESCRT components.[23,24] The ESCRT machinery sorted by Hgs has been shown to play a dual role in limiting intracellular signalling molecule accumulation, by targeting them to MVBs and lysosomes for degradation, but also promoting their secretion.[25–29] *Hgs* deficiency causes motor and sensory deficits, impaired oesophageal motility, and embryonic lethality in mice.[30–32] An *in vitro* study has shown that Hgs is involved in tight junction protein trafficking and EC permeability.[33] Nevertheless, the functions of Hgs or other ESCRT components in EC polarity and cerebrovascular stability have not been explored.

Here, we investigated for the first time whether the ESCRT machinery is required for EC polarity using a mouse model in which *Hgs* was disrupted in cerebrovascular ECs. Mice with *Hgs* knocked out in brain ECs exhibited distorted polarity of ECs and died at birth. We found that knockdown of endothelial Hgs blocked the trafficking of endocytosed VE-cadherin as well as other junctional proteins from early endosomes to recycling endosomes and impaired the motility of recycling endosomes. We further demonstrated that the motor kinesin protein KIF13A could rescue the abrogated polarized distribution of VE-cadherin in Hgs knockdown ECs. These findings reveal an essential role for the ESCRT machinery in the maintenance of EC polarity and cerebrovascular stability.

# 2. Methods

## 2.1 Mice

Mice carrying floxed *Hgs* alleles[32] and *SP-A-Cre* transgenic mice[34–36] have been reported previously. Genotypes of the offspring were determined by PCR using specific primers as follows: *Hgs*; 5′-CCTGGTG TCCTTGGATCTCCT-3′ and 5′-GAGCCACTCTTGTAGCCTTGC-3′, *Cre*; 5′-GCCTGCATTACCGGTCGATGC-3′ and 5′-CAGGGTGT TATAAGCAATCCC-3′. The experiments were performed according to the protocols approved by the Animal Experiment Committee of the Beijing Institute of Lifeomics and conformed to the US National Institutes Guide for the Care and Use of Laboratory Animals. All animals used for experiments were bred into a C57B/L6 background. The pregnant mice were anaesthetized by 2–2.5% isoflurane inhalation in an anaesthesia induction chamber for 2–3 min and then transferred to the animal platform for embryonic dissection or embryonic blood–brain barrier (BBB) permeability assay. During these processes, the pregnant mice were continually anaesthetized by 1–1.5% isoflurane inhalation through anaesthesia masks covering their noses. Following the procedures, the pregnant mice were euthanized by cervical dislocation.

## 2.2 Cell culture and small RNA interference

Human umbilical vein endothelial cells (HUVECs) were isolated as previously described[37] and cultured at 37°C with 5% $CO_2$ in endothelial growth medium EGM2 (LONZA) with the addition of growth supplement, 10% FBS (HyClone), 100 U/mL penicillin, and 100 mg/mL streptomycin. When the cells reached approximately 50% confluency, HUVECs were transfected with siRNA oligonucleotides using jetPRIME (Polyplus) according to the manufacturer's protocol.

The bEnd.3 cell line (ATCC) was cultured at 37°C with 5% $CO_2$ in DMEM with 10% FBS. Gene knockdown was achieved by transfection of the following siRNA oligos: Hgs-siRNA for HUVECs; 5′-GGACCUGC UGAAGAGACAATT-3′ and 5′-GCCUGUACUCUUCACCUGUTT-3′, Hgs-siRNA for bEnd.3 cells; 5′-AUCUGUAGAAUGGACUCCCTT-3′ and 5′-ACAUUAACUUCCACUUGCCTT-3′, KIF13A-siRNA for HUVECs; 5′-GCACUCAUUAAACGACGAGTT-3′ and 5′-CCGCAAC AACUUGGUAGGATT-3′. Experiments were performed 48–72 h after transfection.

## 2.3 Plasmids

The enhanced green fluorescent protein (EGFP)-VE-cadherin plasmid was a gift from Naoki Mochizuki (National Cardiovascular Center Research Institute, Osaka, Japan), and pcDNA3.1 was from Addgene. Human cDNA fragments encoding full-length Rab11a and KIF13A were obtained by RT-PCR and cloned into the pCDNA3.1-mCherry vector and pcDNA3.1(+) vector, respectively.

## 2.4 Immunostaining

Embryonic brains were fixed with 4% paraformaldehyde overnight, embedded in paraffin, and either sectioned at 6 μm or embedded in optimal cutting temperature (OCT, SAKURA) compound and subsequently sectioned at 40 μm. After incubation in blocking serum for 30 min at 37°C, sections were incubated with the following primary antibodies: Hgs (1:300, ab155539, Abcam), VE-cadherin (1:300, ab33168, Abcam), Collagen IV (1:300, ab33168, Abcam), ERG (1:300, ab92513, Abcam), Ki67 (1:300, ab16667, Abcam), PDGFRβ (1:200, 3169, CST), cleaved caspase-3 (1:200, 9661, CST), PARD6A (1:100, SC-365323, Santa Cruz), RhoA (1:100, SC-418, Santa Cruz), PODXL (1:200, AF1556, R&D Systems), CD31 (1:100, 550274, BD), IB4 (1:200, L2140, Sigma-Aldrich), Nectin2 (1:200, 383172, ZENBIO), Claudin-5 (1:200, 35-2500, Invitrogen), and Endomucin (1:100, 4348280, Invitrogen), followed by incubation with fluorescence-conjugated secondary antibodies (1:1000, Alexa Flour 488/568/647, Invitrogen).

HUVECs and bEnd.3 cells grown on glass coverslips were fixed with 4% paraformaldehyde for 20 min, washed with PBS, and permeabilized with 0.5% Triton X-100 for 20 min. After blocking with blocking serum, cells were incubated with the following primary antibodies: Rab5 (1:200, 2143, CST), Rab11 (1:200, 5589, CST), HA-Tag (1:200, 3724, CST), Rab4 (1:200, Abcam, ab109009), Claudin5 (1:200, 352588, Invitrogen), and Phalloidin-Rhodamine (P1951, Sigma-Aldrich), followed by incubation with fluorescence-conjugated secondary antibodies as above.

Samples were sealed in Prolong (Invitrogen) for confocal microscopy analyses.

## 2.5 BBB permeability assay

All embryonic BBB permeability assays were performed blind before genetyping. Pregnant mice were anaesthetized as described in Section 2.1; and dye containing 2% Evans blue was injected into the embryonic liver by using a Hamilton syringe. After perfusion with PBS, embryonic brains were homogenized in formamide at 37°C for 2 h. The concentration of Evans blue was quantified at 620 nm.

To test the barrier function of ECs *in vitro*, a transwell insert (0.4 μm pore, 12 mm diameter, Millipore) was placed above the well of a 24-well culture plate containing 500 μL growth medium, and bEnd.3 cells transfected with control- or Hgs-siRNA in 300 μL growth medium were seeded in the upper compartment. About 1 μL Evans blue dye was added to the upper compartment and the concentration of Evans blue in the growth medium in the lower compartment was subsequently quantified at 620 nm.

## 2.6 Real-time PCR

Total RNAs were isolated from FACS-sorted E14.5 brain ECs using TRIzol Reagent (Life Technologies) according to the manufacturer's instructions. Reverse transcription of mRNA was performed using reverse transcriptase master mix (TOYOBO). *Hgs* expression was measured on the 7500 Fast Real-Time PCR System (Applied Biosystems) using SYBR Green Real-time PCR Master Mix (TOYOBO) according to the manufacturer's instructions. *Gapdh* was used as the internal control. The following primers were used: *Gapdh*; 5′-TGCCCAGAA CATCATCCCT-3′ and 5′-GGTCCTCAGTGTAGCCCAAG-3′, *Hgs*; 5′-CCAATGTCCATGGGCTACCA-3′ and 5′-CTGCTGGTACAGGG GCTG-3′.

## 2.7 Western blots

Protein lysate samples from extracts of bECs and HUVECs were boiled in Laemmli sample buffer, separated using 10% or 12% polyacrylamide gels, and transferred onto polyvinylidene-fluoride (PVDF) membranes (Millipore). Membranes were blocked with 5% milk for 1 h and incubated overnight at 4°C with the following primary antibodies: Hgs (1:1000, ALX-804-382, Enzo), VE-cadherin (1:2000, ab33168, Abcam), Rab4 (1:2000, ab109009, Abcam), Rab5 (1:1000, 2143, CST), Rab11 (1:1000, 5589, CST), KIF13A (1:1000, A301-077A-T, Bethyl Laboratories), and GAPDH (1:1000, TA-08, Zsbio). Membranes were then incubated with horseradish peroxidase-conjugated secondary antibodies and developed using enhanced chemiluminescent (ECL).

## 2.8 AMIS polarity assay

In spreading HUVECs that undergo apical-basolateral polarization, an F-actin-rich bud forms at the apical surface and is the target of polarized trafficking of several proteins, such as VE-cadherin.[38] To create a model for this polarized trafficking, confluent HUVECs were trypsinized in order to separate their cell–cell contacts but still were allowed to adhere on the surfaces of vitronectin-coated glass (Millicell). After removal of trypsin, the cells were allowed to spread in fresh medium at 37°C for 25 min, at which point the cells formed AMIS buds at their apical surface. The cells were then fixed, blocked, permeabilized, and incubated with primary antibodies overnight at 4°C as described in Section 2.4. Following incubation with secondary antibodies, HUVECs were incubated with Phalloidin-Rhodamine (P1951, Sigma-Aldrich) for 1 h at 37°C to label F-actin. Samples were sealed in Prolong (Invitrogen) for confocal microscopy analyses.

## 2.9 Flow cytometry

Embryonic brains were digested in a solution containing 0.2% collagenase H, and 10% bovine serum albumin (BSA) in PBS for 1 h at 37°C. After centrifugation for lipid separation, samples were incubated with CD144-PE and CD45-APC antibodies (eBioscience), and processed for FACS analyses and FACS sorting using standard procedures. Dead cells were excluded using 7-amino-actinomycin D staining.

## 2.10 Internalization assay

HUVECs were cultured on 4-well glass plates (Millicell) and transfected with control- or Hgs-siRNA. After 42 h, cells were incubated for 1 h with fresh growth medium containing antibody of interest (VE-cadherin, V1514, Sigma-Aldrich; CD31, 550389, BD; and Claudin-5, 352588, Invitrogen). After washing with ice-cold PBS to remove unbounded antibodies, HUVECs were incubated with 100 μM chloroquine containing medium for 4 h, and fixed with 4% PFA. The cells were then subject to immunofluorescence stained as described in Section 2.4 and imaged by confocal microscopy.

## 2.11 Microscopy

Confocal microscopy of fixed cells and tissues was performed with a confocal microscope (LSM 880 Airyscan; Zeiss) equipped with Diode (405 nm), Argon (458, 488, and 514 nm), Solid state (561 nm), and HeNe (633 nm) excitation laser lines. Image acquisition was performed using a 63 × 1.4 NA Oil Plan-Apochromat objective, a 40 × 0.75 NA W N-Achroplan (water dipping lense) objective or a 20 × 0.8 NA Plan-Apochromat objective. The confocal software of Zen (Zeiss), and Imaris and ImageJ image analysis softwares were used for data analyses.

## 2.12 Live cell imaging

For live cell imaging, cells transfected with siRNA and DNA plasmids were transferred from 6-well plates to glass-bottomed dishes at 37°C before observation. Live cell imaging of intracellular protein dynamics was performed by spinning disk confocal microscopy (UltraVIEW VoX; PE). Two-colour channels of 8–10 Z-slices were acquired by changing light paths using 70–100 ms exposures for over 10 min per Z-stack under the 'UltraVIEW Focus Drive'. Analyses of the endosome movement speed and tracing pathway were performed using the software Volocity.

## 2.13 Confocal microscopy analysis

### 2.13.1 Relative Hgs intensity

IB4 staining and Hgs staining of 6-μm thick sections were captured at two different coloured channels by confocal microscopy (LSM 880 Airyscan; ZEISS). The Hgs-positive signal both within and outside of IB4-positive vessels were analysed using the integrated density measurement tool in ImageJ software. Relative Hgs intensity was quantified by dividing the Hgs-positive fluorescent signal per unit area in IB4-positive vessels by the Hgs-positive fluorescent signal per unit area outside IB4-positive vessels. Fifteen corresponding areas in five animals of each genotype were analysed.

### 2.13.2 Cerebellar microvessel diameter

To analyse IB4 staining of 40-μm thick sections, images were captured by confocal microscopy, then 10 equidistant parallel lines were set, and the cross-points were selected for vascular diameter analysis by ImageJ

software. Five mice for each genotype and totally 15 sections of each individual were analysed.

#### 2.13.3 Empty sleeves

IB4 staining and collagen IV staining of 40-μm thick sections were captured at two different coloured channels. The 'angiogenesis' plugin in ImageJ software was used to measure the length of IB4-positive vessels and the length of collagen IV-positive vessels, the difference between which was taken as the length of collagen IV-positive, IB4-negative empty endothelial sleeves. Fifteen corresponding areas in five animals of each genotype were analysed.

#### 2.13.4 Percentage of cleaved caspase-3-positive apoptotic ECs and Ki67-positive proliferating ECs

Representative images were acquired by confocal microscopy. The IB4 signal was first subjected to threshold processing and recorded for surface modelling using the 'surface' measurement tool in Imaris software, in order to identify all the vessels. Next, the percentage of cleaved caspase-3-positive apoptotic ECs was calculated by counting the relative proportion of cleaved caspase-3/IB4 double positive cells to DAPI/IB4 double positive cells in each image. The percentage of Ki67-positive proliferating ECs was calculated in the same way. Fifteen corresponding areas in five animals of each genotype were analysed.

#### 2.13.5 Pericyte coverage

For pericyte coverage, PDGFRβ and endomucin signals from microvessels were separately captured. The areas occupied by these two respective signals were analysed using the 'area' measurement tool in ImageJ software. Pericyte coverage was determined as the percentage of PDGFRβ-positive pericyte surface area that was covering the endomucin-positive capillary surface area per field. Three non-adjacent sections randomly selected in each animal were analysed. Five animals per group were analysed.

#### 2.13.6 Size of Rab5-positive endosomes

For quantification of the size of Rab5-positive endosomes, Z-stacks of HUVECs or bEnd.3 cells stained for Rab5 were captured for 3D reconstruction. Next, the 3D image, including the Rab5-positive signal, was subjected to threshold processing and selected for surface analysis in Imaris software. After manually removing aberrant signals and segregating individual signals as required, the size of Rab5-positive endosomes was calculated by Imaris software automatically.

#### 2.13.7 Junctional VE-cadherin

For quantification of the VE-cadherin signal in ECs, sequential Z-sections of VE-cadherin-stained cells were first recorded for 3D reconstruction. We then used the built-in 'surface' rendering tool in Imaris to model and calculate the VE-cadherin signal on whole cells and in the cytoplasm, with the difference between these two values corresponding to the VE-cadherin signal on junctional membranes. Thirty cells in five experiments of each condition were analysed.

#### 2.13.8 Colocalization in internalization assays

For quantifying internalization of proteins, Z-stacks of cells stained for protein of interest (VE-cadherin, CD31, and Claudin-5) and endosomal markers (Rab5, Rab11, and Rab4) were captured by confocal microscopy and the images were subjected to 3D reconstitution with Imaris software. We then used the 'surface' masking tool in Imaris to create precise 3D regions of the internalized antibody signal, which allowed quantification of the signal. The signal of the endosomal marker antibody was selected for surface analysis in a similar way, allowing quantification of the colocalization of proteins of interest with endosomes. Colocalization was calculated by quantifying the relative proportion of the signal of internalized antibodies colocalizing with endosomes to the total signal of internalized antibodies. Thirty cells in five experiments of each condition were analysed.

#### 2.13.9 Colocalization in AMIS assays

For quantification of colocalization for the AMIS assay, sequential Z-sections of stained cells were recorded for 3D reconstruction. First, the signal of polarity proteins (VE-cadherin, CD31, and Claudin-5) on a whole EC was subjected to threshold processing and masked using the 'surface' measurement tool in Imaris, allowing automatic quantification of the signal. Next, the region of AMIS buds was masked using the 'surface' measurement tool. Within this region, the 'channel masking' technique was used to identify the Rab11-positive recycling endosomes within AMIS buds. Then, the 'channel masking' technique was used again to mask the polarity protein signals within the Rab11-positive recycling endosomes in the AMIS buds. Finally, the colocalization was quantified by counting the relative proportion of polarity protein signal within Rab11-positive recycling endosomes of the AMIS buds to the total signal of each polarity protein. Thirty cells in five experiments of each condition were analysed.

### 2.14 Statistical analysis

The Mann–Whitney test or one-way analysis of variance was used for statistical analysis of two groups of samples or multiple groups of samples, respectively. The error bars on graphs represent the mean ± standard deviation. $*P < 0.05$ and $**P < 0.01$ were taken to be statistically significant.

## 3. Results

### 3.1 Deletion of *Hgs* in brain ECs disrupts cerebrovascular stability

To investigate the role of Hgs in cerebrovascular development, we bred $Hgs^{flox/flox}$ mice[32] with *SP-A-Cre* transgenic mice,[34–36] in which the Cre recombinase was specifically expressed in brain ECs beginning at E11.5. No obvious difference was observed among littermate wild type, $Hgs^{flox/flox}$, and *SP-A-Cre;* $Hgs^{flox/+}$ (hereafter referred to as control) mice in this study. Immunostaining analyses and quantification confirmed that *Hgs* was deleted in brain ECs of *SP-A-Cre;* $Hgs^{flox/flox}$ (hereafter referred to as $Hgs^{bEC\text{-}KO}$) mice at E14.5 (*Figure 1A* and *B*), which was further verified by real-time PCR analyses of FACS-sorted ECs (*Figure 1C*). A total of 47 offspring at postnatal day 0 (P0) and 294 offspring at P1 or later were genotyped from the *SP-A-Cre;* $Hgs^{flox/+}$ and $Hgs^{flox/flox}$ intercross, and no $Hgs^{bEC\text{-}KO}$ pups were found. However, of 52 offspring analysed at embryonic day 19.5 (E19.5), 7 live $Hgs^{bEC\text{-}KO}$ embryos were detected, indicating that $Hgs^{bEC\text{-}KO}$ mice died between E19.5 and birth, at P0 (*Table 1*). $Hgs^{bEC\text{-}KO}$ embryos displayed enlarged cerebral ventricles and loss of brain parenchyma (Supplementary material online, *Figure S1A*). By visualizing the cerebral vasculatures by whole-mount isolectin B4 (IB4) immunostaining, we found that $Hgs^{bEC\text{-}KO}$ embryos exhibited a dramatic

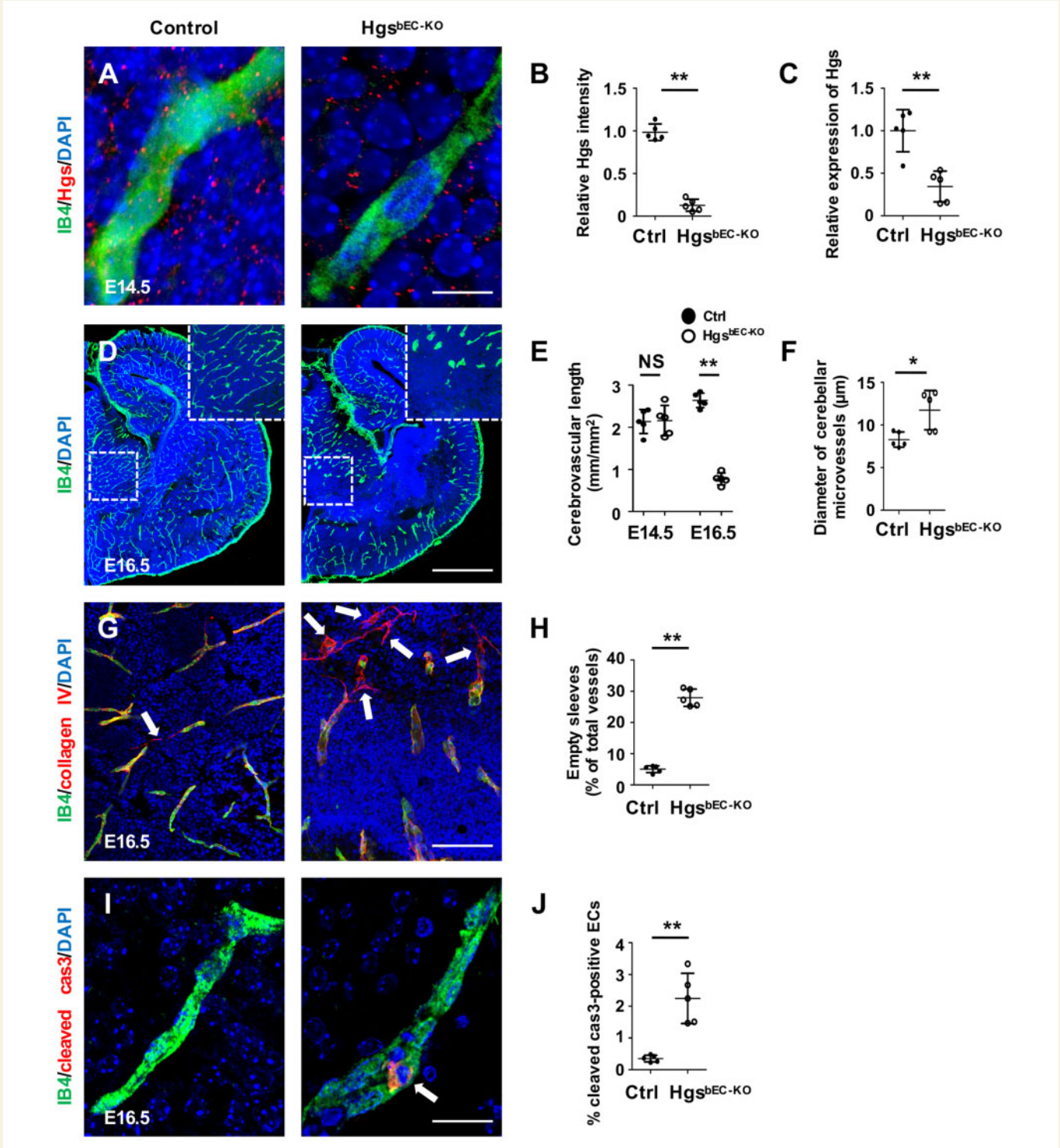


**Figure 1** Deletion of *Hgs* in brain ECs disrupts cerebrovascular stability. (*A*) Hgs and IB4 immunostaining on brain sections of E14.5 control and $Hgs^{bEC\text{-}KO}$ embryos showing the absence of Hgs in $Hgs^{bEC\text{-}KO}$ mutant brain ECs. Scale bar: 15 µm. (*B*) Quantification showing a significant decrease of relative Hgs intensity in IB4-positive vessels vs. Hgs intensity outside IB4-positive vessels in $Hgs^{bEC\text{-}KO}$ mice ($n = 5$). (*C*) Real-time PCR analyses of *Hgs* expression in primary isolated brain ECs derived from E14.5 control and $Hgs^{bEC\text{-}KO}$ embryos ($n = 5$). (*D*) IB4 immunostaining of brain vasculature showing abnormal capillary morphology in $Hgs^{bEC\text{-}KO}$ embryos at E16.5. Scale bar: 800 µm. (*E*) Quantification of brain vasculature density in control and $Hgs^{bEC\text{-}KO}$ embryos at E14.5 and E16.5 ($n = 5$). (*F*) Quantification of the brain microvascular diameters in control and $Hgs^{bEC\text{-}KO}$ embryos at E16.5. (*G*) IB4 and collagen IV immunostaining showing increased brain vascular regression in E16.5 $Hgs^{bEC\text{-}KO}$ embryos. Arrows indicate collagen IV-positive, IB4-negative empty endothelial sleeves. Scale bar: 100 µm. (*H*) Quantification of empty endothelial sleeves in brains of E16.5 control and $Hgs^{bEC\text{-}KO}$ embryos ($n = 5$). (*I*) Cleaved-caspase 3 (cleaved cas3) immunostaining showing an apoptotic brain EC (arrow) in an E16.5 $Hgs^{bEC\text{-}KO}$ embryo. Scale bar: 25 µm. (*J*) Quantification indicating increased apoptotic ECs in brains of E16.5 $Hgs^{bEC\text{-}KO}$ mutants ($n = 5$). Values are presented as means ± standard deviation. $^*P < 0.05$; $^{**}P < 0.01$ and NS, not significant ($P \geq 0.05$) by Mann–Whitney test.

**Table 1 Genotypes of offspring from *SP-A-Cre*; *Hgs*$^{flox/+}$ and *Hgs*$^{flox/flox}$ intercross**

| Age | Embryos by genotype, *n* (%) | | | | Total embryos (*n*) |
|---|---|---|---|---|---|
| | Cre-negative | | Cre-positive | | |
| | flox/+ | flox/flox | flox/+ | flox/flox | |
| E14.5 | 34 (23.6) | 40 (27.8) | 33 (22.9) | 37 (25.7) | 144 |
| E16.5 | 38 (22.1) | 44 (25.6) | 41 (23.8) | 49 (28.5) | 172 |
| E18.5 | 10 (22.2) | 12 (26.7) | 9 (20.0) | 14 (31.1) | 45 |
| E19.5 | 13 (25.0) | 18 (34.6) | 14 (26.9) | 7 (13.5) | 52 |
| P0 | 16 (34.1) | 12 (25.5) | 19 (40.4) | 0 (0) | 47 |
| P1∼ | 105 (35.7) | 90 (30.6) | 99 (33.7) | 0 (0) | 294 |

decrease in capillary density and an increase in microvascular diameter of cerebral vasculatures at E16.5 (*Figure 1D–F*). To examine the stability of Hgs$^{bEC-KO}$ mutant cerebral vasculatures, type IV collagen and IB4 immunostaining were performed to visualize empty endothelial sleeves. We found that the number of empty endothelial sleeves characterized by expression of collagen IV and absence of IB4 was significantly increased in brain vessels of E16.5 Hgs$^{bEC-KO}$ embryos compared to that of controls (*Figure 1G* and *H*), indicating collapsed brain vessels in Hgs$^{bEC-KO}$ mutant embryos. Consistently, endothelial apoptosis indicated by cleaved caspase-3 immunostaining, was significantly increased in Hgs$^{bEC-KO}$ embryos (*Figure 1I* and *J*). In addition, the integrity of the BBB was disrupted in Hgs$^{bEC-KO}$ embryos at E16.5, as demonstrated by widespread blue staining after Evans blue injection (Supplementary material online, *Figure S1B* and *C*). These results suggested that loss of brain endothelial *Hgs* leads to impaired cerebral vasculature stabilization. Analyses of E14.5 Hgs$^{bEC-KO}$ and control embryos showed comparable morphology (Supplementary material online, *Figure S2A*), capillary density or diameter of cerebrovascular vessels (*Figure 1E* and Supplementary material online, *Figure S2B*), PDGFRβ-positive mural cell coverage (Supplementary material online, *Figure S2C* and *D*), empty endothelial sleeves (Supplementary material online, *Figure S2E* and *F*), or the numbers of Ki67-positive proliferating ECs (Supplementary material online, *Figure S2G* and *H*), confirming that endothelial Hgs is likely required for the maintenance of cerebrovascular vessel stability.

## 3.2 Loss of brain endothelial *Hgs* impairs EC polarity

Strikingly, we observed occlusion of vascular lumens and clustered ECs in brain vessels of Hgs$^{bEC-KO}$ mutant embryos, both of which are associated with abnormal EC polarity. During the establishment of EC polarity, formation of the apical surface is dependent on the precise localization of VE-cadherin, which determines the accurate translocation of other polarity-associated proteins such as PODXL, Par6, and the small GTPase protein RhoA.[39] At E16.5, VE-cadherin was appropriately localized along the cell–cell junctional membranes of control brain ECs, but significantly decreased at the junctional membranes of ECs in Hgs$^{bEC-KO}$ mutant embryos (*Figure 2A*). Although western blot analyses of isolated brain ECs showed similar expression of VE-cadherin in brain ECs of Hgs$^{bEC-KO}$ embryos compared with that of controls (*Figure 2B*), flow cytometry analyses revealed significantly decreased mean fluorescence intensity of membranous VE-cadherin in Hgs$^{bEC-KO}$ embryos (*Figure 2C*). As expected, PODXL, an apical cell surface marker, was enriched along the apical membranes of control brain vessels, but lost its polarized distribution in clustered brain ECs of Hgs$^{bEC-KO}$ embryos (*Figure 2D*). Similarly, the polarized distribution of the cell polarity regulators Par6 and RhoA was also impaired in brain ECs of Hgs$^{bEC-KO}$ mutants (*Figure 2E* and *F*). Moreover, two other endothelial adhesion junctional proteins, platelet–endothelial adhesion molecule-1 (PECAM1/CD31), and Nectin-2, lost their polarized distribution in brain ECs of Hgs$^{bEC-KO}$ embryos (Supplementary material online, *Figure S3A* and *B*). Tight junction organization was also disrupted in brain ECs of E16.5 Hgs$^{bEC-KO}$ embryos, as evidenced by incorrectly polarized localization of Claudin-5 (Supplementary material online, *Figure S3C*). These results suggest that deletion of *Hgs* results in defective polarity of cerebrovascular ECs.

## 3.3 Hgs knockdown impairs recycling of endothelial junctional proteins to the plasma membrane *in vitro*

Since the trafficking of VE-cadherin is important in determining the proper distribution of VE-cadherin on the cell membrane, we next investigated whether Hgs regulated the endocytic trafficking of VE-cadherin *in vitro*. Consistent with the observation in Hgs$^{bEC-KO}$ mutant brain ECs, the protein level of VE-cadherin was not affected in Hgs-siRNA-treated HUVECs (Supplementary material online, *Figure S4E*). Compellingly, *z*-axis images of HUVECs showed that depletion of Hgs led to an increased cytoplasmic accumulation of VE-cadherin (*Figure 3A*), accompanied by a decrease in VE-cadherin at the junctional membranes of adjacent HUVECs (*Figure 3C*). Immunostaining in HUVECs showed that Hgs colocalized with Rab5 and Rab11, markers of early and slow recycling endosomes, respectively (Supplementary material online, *Figure S4A* and *B*), while little Hgs colocalized with Rab4, a marker of fast recycling endosomes (Supplementary material online, *Figure S5A*). Knockdown of Hgs did not affect the expression level of Rab5 (Supplementary material online, *Figure S4C*), Rab11 (Supplementary material online, *Figure S4D*), or Rab4 (Supplementary material online, *Figure S5B*). Strikingly, cytoplasmic accumulation of VE-cadherin predominantly occurred in Rab5-positive early endosomes (*Figure 3B*). In addition, the size of Rab5-positive early endosomes was increased in Hgs-depleted cells (*Figure 3D*). We also suppressed Hgs expression by siRNA in an immortalized mouse brain microvessel EC line, bEnd.3, which displays basic characteristics of cerebral microvascular ECs.[40] Consistently, the junctional distribution of VE-cadherin was decreased in Hgs knockdown bEnd.3 cells (Supplementary material online, *Figure S6A* and *B*), accompanied by an accumulation in enlarged Rab5-positive early endosomes (Supplementary material online, *Figure S6A* and *C*).

We further investigated the endocytic trafficking of VE-cadherin using an internalization assay. HUVECs transfected with control- or Hgs-siRNA were labelled with VE-cadherin antibody for 1 h as previously described.[41] After 4 h incubation with 100 μM chloroquine, which blocks the lysosomal degradation pathway, double immunostaining of Rab5 and VE-cadherin revealed the accumulation of VE-cadherin in Rab5-positive early endosomes (siHgs-1; 36.5 ± 3.8% and siHgs-2; 34.5 ± 1.6% versus control; 7.4 ± 0.7%; $P < 0.01$; *Figure 3E* and *H*). Unexpectedly, the accumulation of VE-cadherin in Rab5-positive early endosomes in Hgs-depleted ECs did not result in the subsequent enrichment of VE-cadherin in recycling endosomes, as the percentage of VE-cadherin in Rab11-positive recycling endosomes was markedly decreased in Hgs knockdown ECs (control; 17.81 ± 0.9% vs. siHgs-1; 10.0 ± 0.5% and

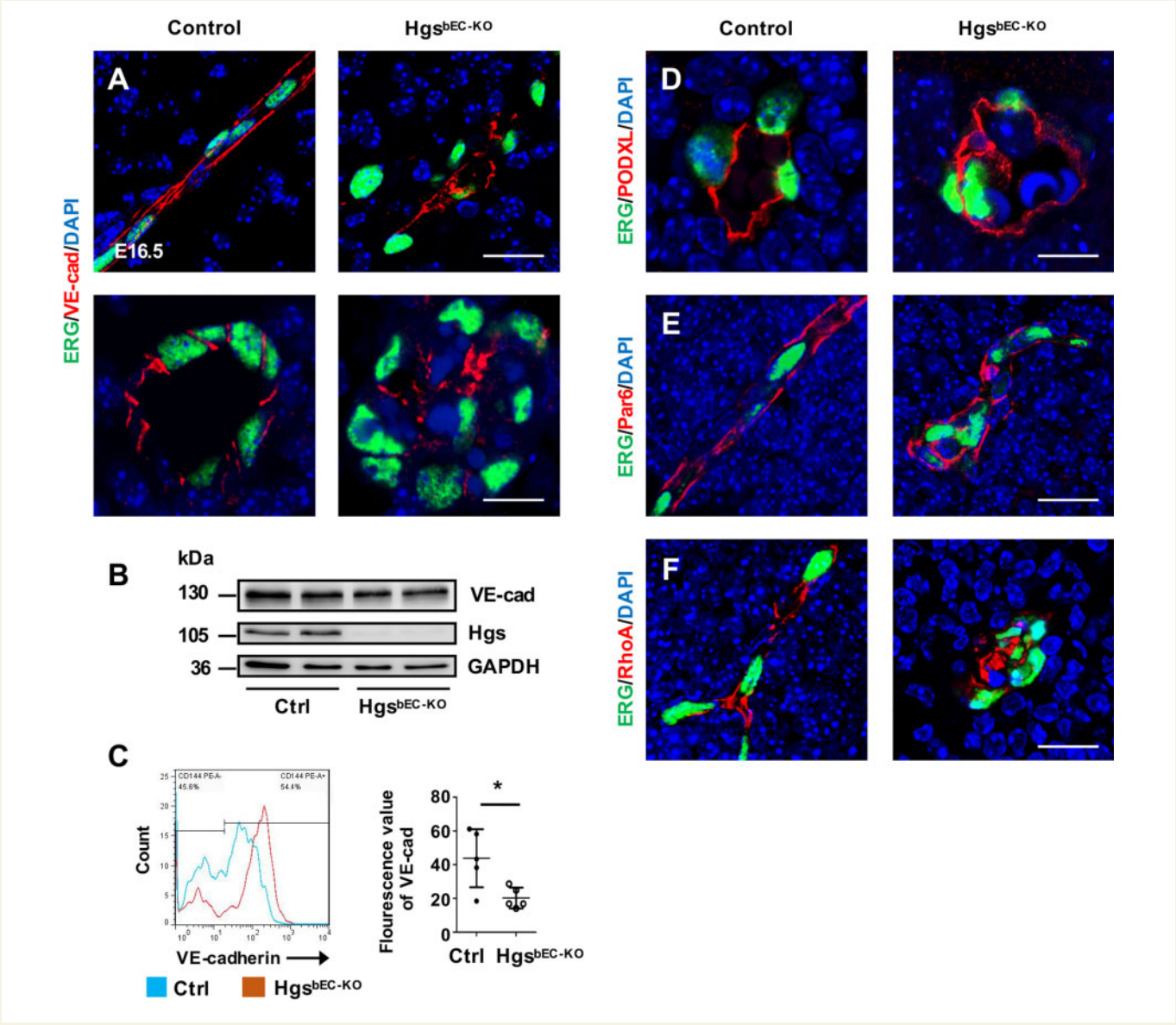


**Figure 2** Loss of brain endothelial *Hgs* impairs EC polarity. (*A*) Confocal images of ERG and VE-cadherin double immunostaining on transverse sections (upper panel) and coronal sections (lower panel) showing the loss of lateral distribution of VE-cadherin in E16.5 $Hgs^{bEC\text{-}KO}$ brain ECs. Scale bar: 20 μm (upper panel) and 10 μm (lower panel). (*B*) Western blot analyses of Hgs and VE-cadherin expression in isolated brain ECs of E16.5 control and $Hgs^{bEC\text{-}KO}$ embryos. (*C*) Flow cytometry analyses of membranous VE-cadherin and the quantification showing a decreased fluorescence intensity in brain ECs of $Hgs^{bEC\text{-}KO}$ embryos compared with controls at E16.5 ($n = 5$). (*D*) Confocal images of PODXL immunostaining showing the disordered apical surface in the clustered brain ECs of E16.5 $Hgs^{bEC\text{-}KO}$ embryos. Scale bar: 10 μm. (*E* and *F*) Confocal images of mislocalized Par6 (*E*) and RhoA (*F*) in brain ECs of $Hgs^{bEC\text{-}KO}$ mice at E16.5. Scale bar: 20 μm. Values are presented as means ± standard deviation. *$P < 0.05$ by Mann–Whitney test.

siHgs-2; 9.2 ± 0.8%; $P < 0.01$; *Figure 3F* and *I*). The percentage of VE-cadherin in Rab4-positive recycling endosomes of Hgs knockdown HUVECs was comparable to controls (Supplementary material online, *Figure S5C*), suggesting that loss of Hgs did not affect Rab4-mediated fast endocytic recycling of VE-cadherin in ECs. Similar results were observed in Hgs knockdown bEnd.3 cells (Supplementary material online, *Figure S6D–G*), indicating that the trafficking of endocytic VE-cadherin from early endosomes to recycling endosomes might be blocked in Hgs knockdown ECs.

We confirmed this observation using an *in vitro* AMIS model. It has been proposed that trafficking of endocytic VE-cadherin to the AMIS represents an initial step to drive apicobasal polarity.[38] Immunostaining revealed that Rab11-positive recycling endosomes were localized at the AMIS, while Rab4-positive recycling endosomes were localized under the AMIS (Supplementary material online, *Figure S5D*). Knockdown of Hgs decreased the enrichment of Rab11-positive recycling endosomes in the AMIS but did not affect the distribution of Rab4-positive recycling endosomes (Supplementary material online, *Figure S5D*). Knockdown of Hgs also significantly reduced the enrichment of VE-cadherin in Rab11-positive recycling endosomes at the AMIS (*Figure 3G* and *J*), demonstrating that recycling of VE-cadherin to the plasma membrane is impaired in Hgs-depleted ECs.

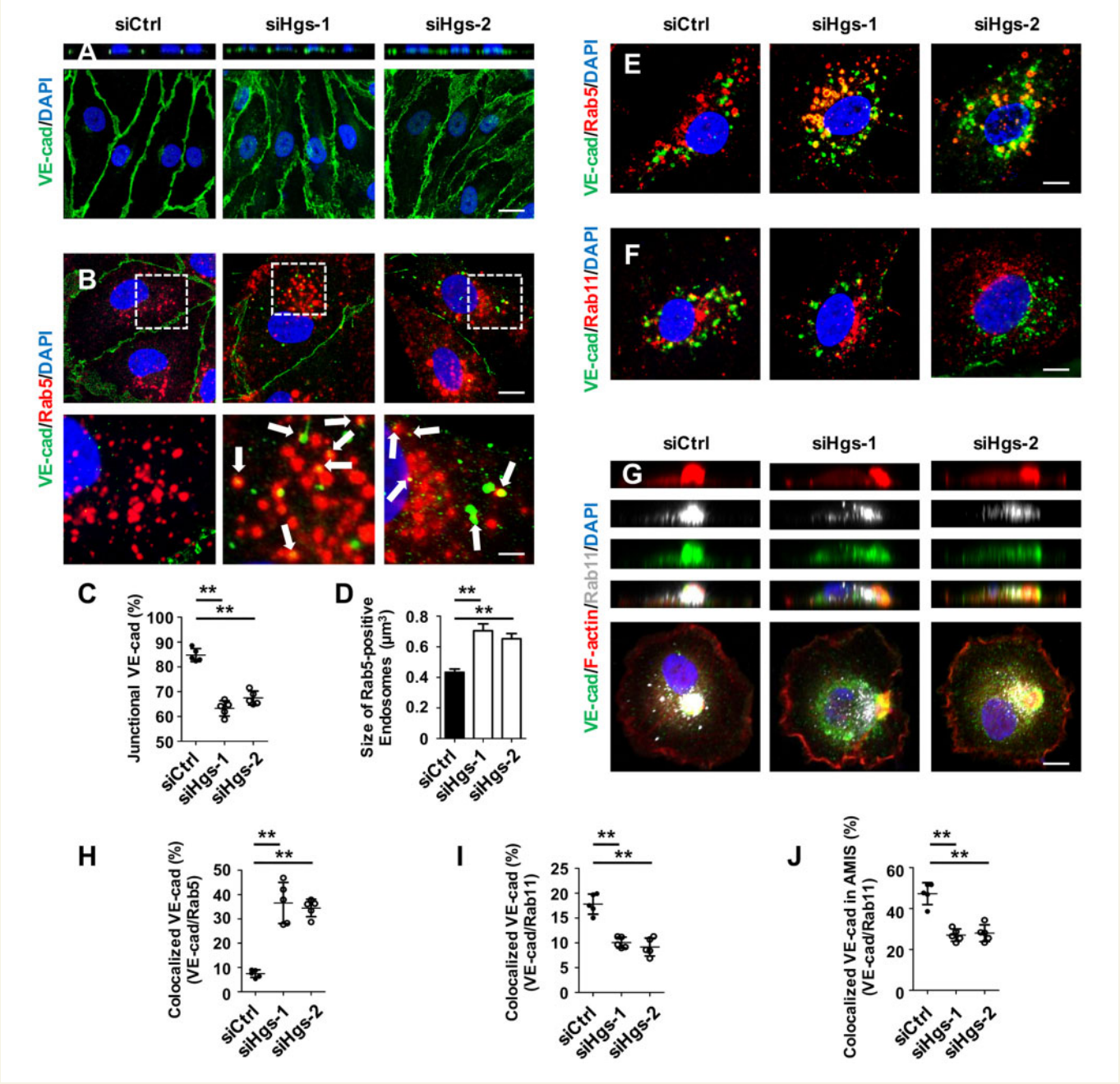


**Figure 3** Hgs knockdown impairs recycling of VE-cadherin to the plasma membrane. (*A–J*) HUVECs were treated with control or Hgs-siRNA for 48 h before fixation in 4% PFA. (*A*) Immunostaining of VE-cadherin showing an increased cytoplasmic accumulation and a loss of polarized distribution in Hgs knockdown HUVECs. Scale bar: 20 μm. (*B*) Double immunostaining of Rab5 and VE-cadherin showing colocalization of internalized VE-cadherin with Rab5-positive early endosomes (arrows) in siHgs-treated HUVECs. Scale bar: 10 μm (upper panel) and 3 μm (lower panel). (*C*) Quantification of junctional VE-cadherin indicating a decreased junctional distribution in Hgs knockdown HUVECs ($n = 5$). (*D*) Quantification of the size of Rab5-positive early endosomes showing a 1.6-fold and a 1.5-fold increase in Hgs knockdown HUVECs (932 endosomes from controls, 886 endosomes from siHgs-1-treated HUVECs, and 804 endosomes from siHgs-2-treated HUVECs were analysed). (*E*) VE-cadherin internalization assay showing the increased colocalization of internalized VE-cadherin with Rab5-positive early endosomes in Hgs knockdown ECs. HUVECs were incubated with VE-cadherin antibody for 1 h and then treated with 100 μM chloroquine for 4 h. Scale bar: 10 μm. (*F*) VE-cadherin internalization assay showing the decreased colocalization of internalized VE-cadherin with Rab11-positive recycling endosomes in Hgs knockdown ECs. Scale bar: 10 μm. (*G*) Immunostaining showing decreased VE-cadherin enrichment at the F-actin bud of AMIS, indicating the impaired recycling of VE-cadherin to the plasma membrane in Hgs knockdown HUVECs. Scale bar: 10 μm. (*H*) Quantification of VE-cadherin/Rab5 colocalization in VE-cadherin internalization assays of control and Hgs knockdown HUVECs ($n = 5$). (*I*) Quantification of VE-cadherin/Rab11 colocalization in VE-cadherin internalization assays of control and Hgs knockdown HUVECs ($n = 5$). (*J*) Quantification of the enrichment of VE-cadherin in Rab11-positive recycling endosomes at the AMIS bud in control and Hgs knockdown HUVECs ($n = 5$). Values are presented as means ± standard deviation. $^{**}P < 0.01$ by Mann–Whitney test.

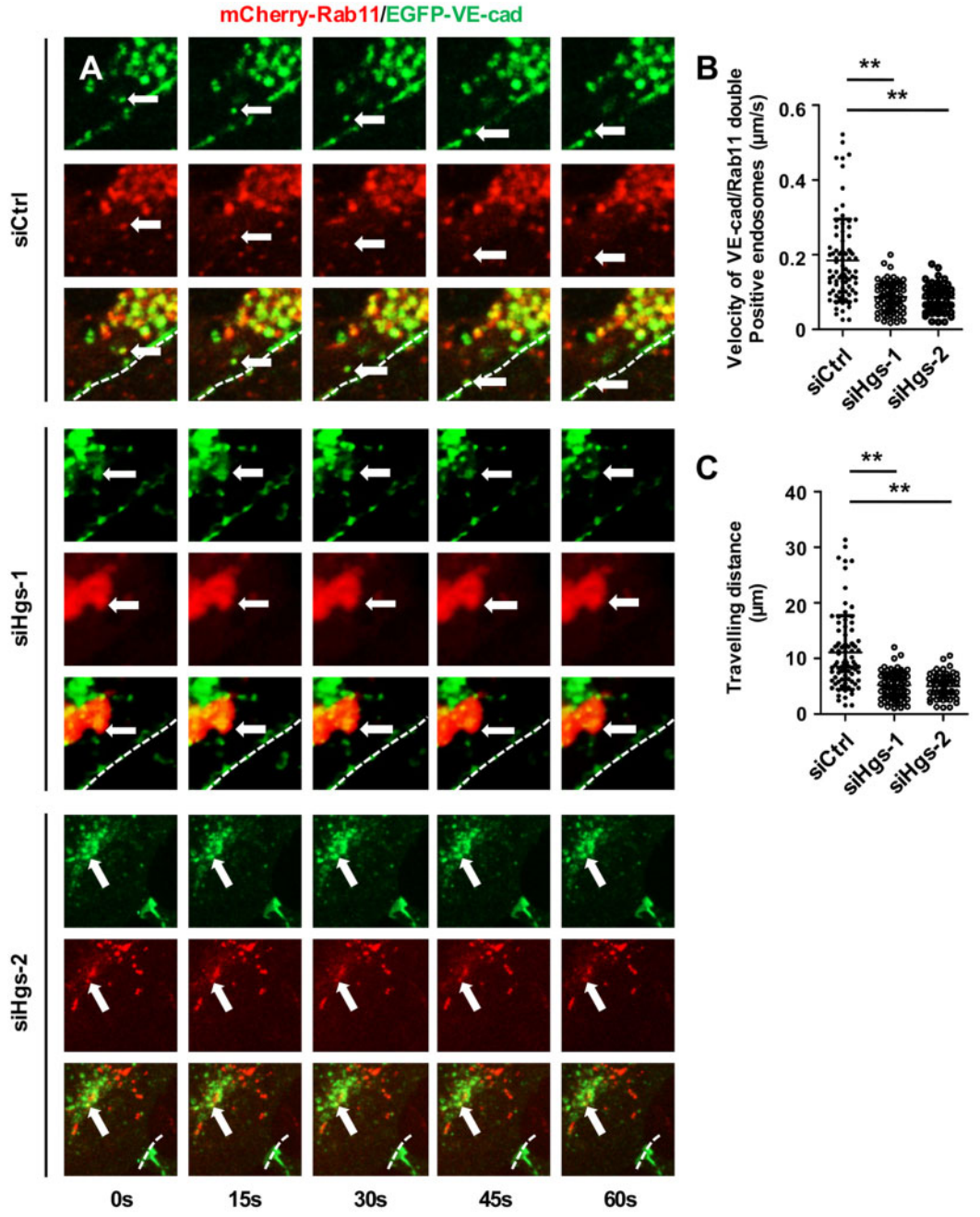


**Figure 4** Hgs knockdown impairs recycling endosome motility in ECs. (*A*) Representative recordings of an imaging series of recycling endosomes marked by mCherry-Rab11 and EGFP-VE-cadherin in control and Hgs knockdown HUVECs treated with siRNA for 48 h and plasmids for 24 h. Arrows indicate the Rab11 and VE-cadherin double positive vesicles at the indicated time points. Dashed lines indicate the junctional contact between two HUVECs. (*B*) Quantification revealed the decreased movement speed of VE-cadherin-containing recycling endosomes in Hgs knockdown HUVECs (84 endosomes from control HUVECs, 77 endosomes from siHgs-1-treated HUVECs, and 63 endosomes from siHgs-2-treated HUVECs were analysed from 4 to 5 different movies). (*C*) Quantification showing decreased travelling distance of VE-cadherin-containing recycling endosomes within 1 min in Hgs knockdown HUVECs (84 endosomes from control HUVECs, 77 endosomes from siHgs-1-treated HUVECs, and 63 endosomes from siHgs-2-treated HUVECs were analysed from 4 to 5 different movies). Values are presented as means ± standard deviation. $^{**}P < 0.01$ by Mann–Whitney test.

We next investigated the role of Hgs in the translocation of VE-cadherin-containing recycling endosomes to the EC membrane. We knocked down Hgs in HUVECs transfected with both EGFP-VE-cadherin and mCherry-Rab11 expression constructs. Time-lapse imaging revealed that depletion of Hgs led to a significant decrease in the movement speed of VE-cadherin-containing recycling endosomes (control; 0.185 ± 0.012 μm/s vs. siHgs-1; 0.087 ± 0.004 μm/s and siHgs-2; 0.185 ± 0.012 μm/s; $P < 0.01$; *Figure 4A* and *B*; Supplementary material

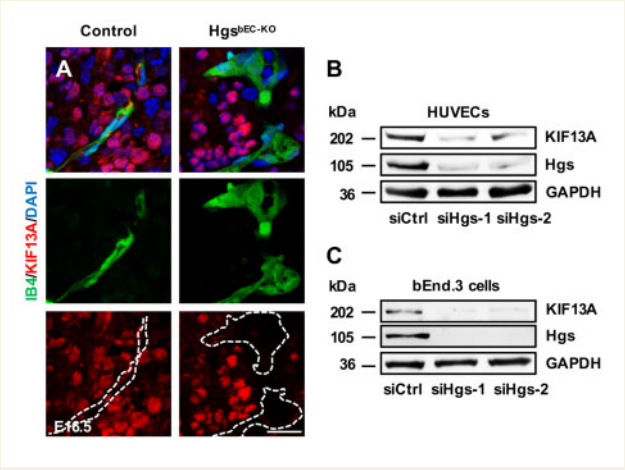


**Figure 5** KIF13A expression is decreased in *Hgs* knockout mouse brain and Hgs knockdown ECs. (*A*) IB4 and KIF13A immunostaining on brain sections of E16.5 control and Hgs$^{bEC-KO}$ embryos showing decreased KIF13A expression in mutant brain ECs. Scale bar: 20 μm. (*B* and *C*) Western blot analyses of Hgs and KIF13A expression in HUVECs (*B*) and bEnd.3 cells (*C*) transfected with control- or Hgs-siRNA.

online, *Movies S1–S3*). Consistently, tracing the paths of VE-cadherin-containing recycling endosomes within 1 min confirmed the impaired movement of VE-cadherin-containing recycling endosomes (*Figure 4C*).

To check whether the trafficking of other junctional proteins was affected in a similar manner, we detected the trafficking of CD31 and Claudin-5 in HUVECs following Hgs depletion. The junctional distribution of CD31 and Claudin-5 was decreased on the membrane, where as their accumulation in enlarged Rab5-positive early endosomes was increased in Hgs knockdown ECs (Supplementary material online, *Figure S3D*, *H*, *L*, and *P*). In the internalization assay and the AMIS model, knockdown of Hgs impaired the trafficking of endocytic CD31 and Claudin-5 from early endosomes to recycling endosomes, and from recycling endosomes to the cell membrane, respectively (Supplementary material online, *Figure S3E–G*, *I–K*, *M–O*, and *Q–S*), suggesting a critical role of Hgs in the recycling of junctional proteins in ECs.

Altogether, these data suggest that Hgs is involved in recycling junctional proteins, including VE-cadherin, back to the EC membrane, by regulating both trafficking from the early endosomes to recycling endosomes and the translocation of recycling endosomes to the cell membrane.

### 3.4 Restoration of endosomal recycling rescues polarized distribution of VE-cadherin in Hgs knockdown ECs

KIF13A, a plus-end-directed microtubule motor protein that belongs to the kinesin-3 subfamily, provides driving force essential for the separation of recycling endosomes from early endosomes, thereby contributing to the endosomal recycling of several membrane proteins.[18,42] To investigate whether KIF13A is involved in Hgs-mediated endosomal recycling of VE-cadherin, we measured the expression of KIF13A in brain ECs of control and Hgs$^{bEC-KO}$ mutant embryos at E16.5. As shown in *Figure 5A*, the expression of KIF13A protein was significantly decreased in ECs of Hgs$^{bEC-KO}$ embryos compared to control embryos. Consistently, western blot analyses showed that Hgs knockdown decreased KIF13A expression in HUVECs and bEnd.3 cells (*Figure 5B* and *C*). Knockdown of KIF13A led to a decrease in VE-cadherin at the junctional membrane accompanied by an accumulation of VE-cadherin in enlarged Rab5-positive early endosomes (*Figure 6A* and *B*) but had no effect on the expression level of VE-cadherin (*Figure 6C*). In the internalization assay and the AMIS model, knockdown of KIF13A led to impaired endocytic VE-cadherin recycling from early endosomes to recycling endosomes and from recycling endosomes to the membrane, respectively (*Figure 6D–H*), indicating a critical role for KIF13A in the endocytic recycling of VE-cadherin to the plasma membrane of ECs.

Next, we investigated whether reinforcing the recycling of endosomes by KIF13A overexpression could rescue the aberrant VE-cadherin polarity in Hgs knockdown ECs. KIF13A expression markedly reduced the accumulation of VE-cadherin-containing Rab5-positive early endosomes and the average size of early endosomes in Hgs knockdown HUVECs (*Figure 7A* and *B*) and bEnd.3 cells (Supplementary material online, *Figure S6H* and *I*). In addition, the junctional distribution of VE-cadherin was restored by KIF13A overexpressing in Hgs knockdown HUVECs (*Figure 7C*) and bEnd.3 cells (Supplementary material online, *Figure S6J* and *K*). Furthermore, overexpression of KIF13A significantly increased the abundance of VE-cadherin at the AMIS in Hgs knockdown HUVECs (*Figure 7D*). These results indicate that endosomal recycling of VE-cadherin is important for maintaining polarized distribution of VE-cadherin in ECs.

## 4. Discussion

To our knowledge, our study is the first to uncover an important physiological function of the Hgs-regulated ESCRT machinery in the maintenance of EC polarity and cerebrovascular stability. Previous studies have demonstrated that ESCRT machinery functions in cellular polarity of epithelial cells and fibroblasts. In *Drosophila*, mutants of *erupted* and *VPS25*, two components of ESCRT-I and ESCRT-II, display defective polarity of epithelial cells.[43,44] In canine kidney cells, depletion of *Tsg101*, the human orthologue of *erupted*, results in the loss of epithelial cell polarity and the intercellular accumulation of tight junction protein claudin-1.[22] In humans, the ESCRT machinery is required for polarization of fibroblasts by regulating integrin trafficking to activate myosin light-chain kinase.[21] In the current study, we investigated the consequences of disturbing ESCRT function on EC polarity by knocking out *Hgs* in cerebrovascular ECs. We showed that deletion of brain endothelial *Hgs* led to the disruption of EC polarity, as evidenced by the mislocalization of polarized EC apical marker, cell–cell junction molecules, and polarity determinants. The density of brain vessels of *Hgs* conditional knockout embryos was comparable with that of control embryos at E14.5. However, collapsed cerebral vasculatures accompanied by an increase in apoptotic ECs and excessive vessel regression were observed in Hgs$^{bEC-KO}$ mutant embryos at E16.5, suggesting that Hgs-regulated ESCRT machinery is required for maintaining cerebrovascular stability.

Our data suggest that Hgs-mediated ESCRT pathway maintains EC polarity via regulating the recycling of endothelial adhesion junctional proteins, including VE-cadherin, to the plasma membrane. Hgs is essential for recognizing and sorting the ubiquitinated cargos from early endosomes to MVBs for degradation. Knockdown of *Hgs* in epithelial cells results in the accumulation of several membrane proteins, such as Smoothened, Frizzled, and connexin-43 in early endosomes and the

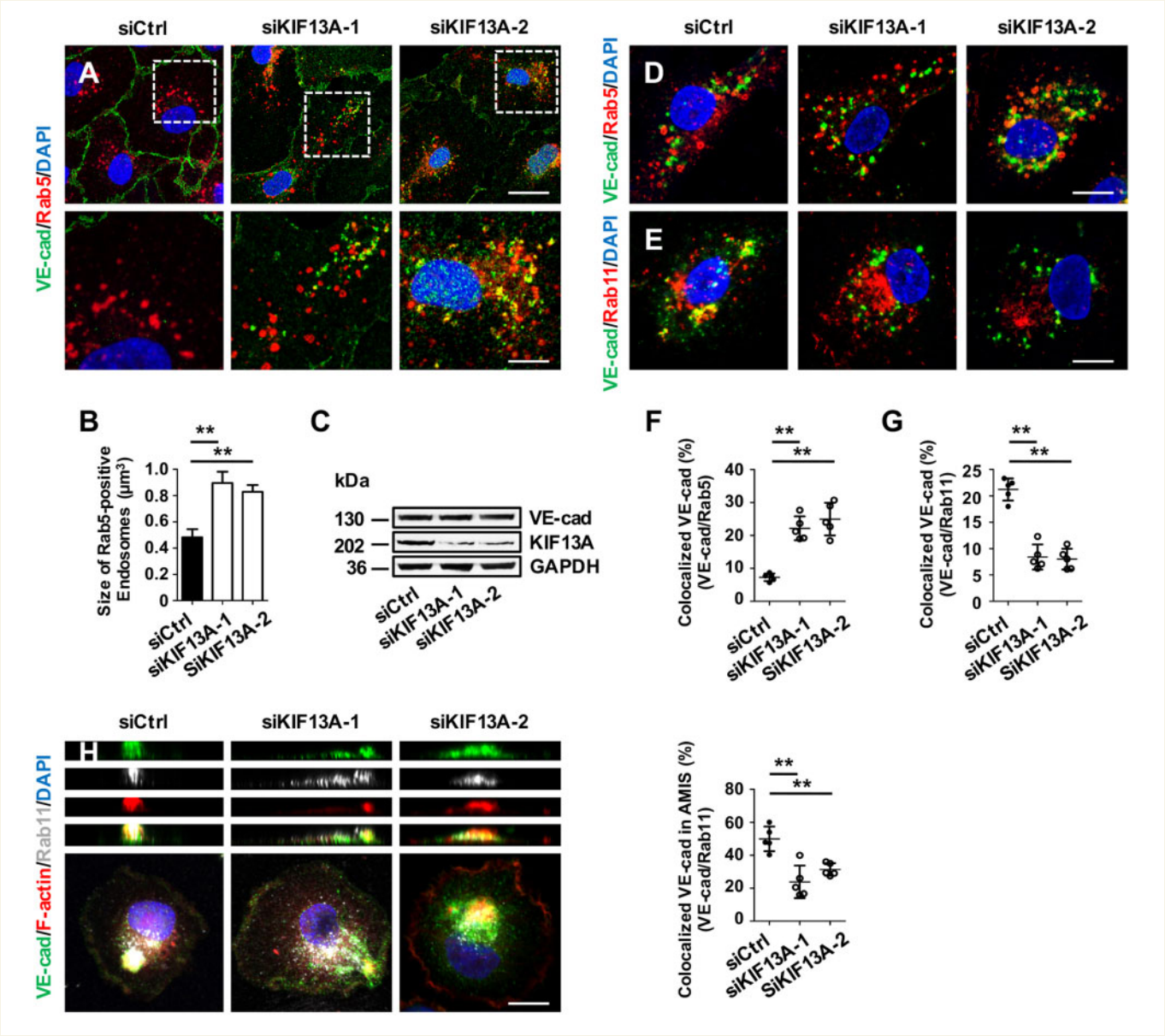


**Figure 6** KIF13A knockdown impairs endocytic recycling of VE-cadherin in ECs. (*A*) Confocal images of VE-cadherin and Rab5 double immunostained HUVECs showing increased VE-cadherin/Rab5 double positive early endosomes in KIF13A knockdown HUVECs. Scale bar: 20 μm (upper panel) and 8 μm (lower panel). (*B*) Quantification showing increased size of Rab5-positive early endosomes in KIF13A knockdown HUVECs (266 endosomes from control HUVECs, 289 endosomes from siHgs-1-treated HUVECs, and 275 endosomes from siHgs-2-treated HUVECs were analysed). (*C*) Western blot analyses of VE-cadherin and KIF13A expression in control and KIF13A knockdown HUVECs. (*D*–*G*) VE-cadherin internalization assay (*D* and *E*) and the corresponding quantifications (*F* and *G*) showing increased colocalization of VE-cadherin with Rab5-positive early endosomes and decreased colocalization of VE-cadherin with Rab11-positive recycling endosomes in KIF13A knockdown HUVECs ($n = 5$). Scale bars: 15 μm. (*H*) Immunostaining for VE-cadherin, Rab11, and F-actin showing impaired recruitment of VE-cadherin-containing recycling endosomes to the AMIS of KIF13A knockdown HUVECs. (Right) Quantification of VE-cadherin/Rab11-positive endosomes enriched at the AMIS of control and KIF13A knockdown HUVECs ($n = 5$). Scale bar: 15 μm. Values are presented as means ± standard deviation. $^{**}P < 0.01$ by Mann–Whitney test.

blocked trafficking to lysosomes.[45–47] In ECs stimulated by vascular endothelial growth factor (VEGF), the ubiquitinated tight junctional protein occludin traffics from the cell border to Hgs-positive punctations and interacts with Hgs, indicating that Hgs plays a role in EC permeability.[33] In this study, we found that Hgs is required for the recycling of endothelial adhesion junctional proteins, including VE-cadherin, to the plasma membrane. The restricted localization of VE-cadherin at the junctional membranes of brain ECs was disrupted in $Hgs^{bEC\text{-}KO}$ mice. Consistently, depletion of Hgs in HUVECs blocked trafficking of endocytosed VE-cadherin from early endosomes to recycling endosomes, leading to cytoplasmic accumulation of VE-cadherin and a consequent decrease of VE-cadherin at the junctional membrane. Supportively, loss of Hgs greatly reduced the enrichment of VE-cadherin-containing recycling endosomes at the AMIS, confirming that Hgs plays a critical role in the recycling of

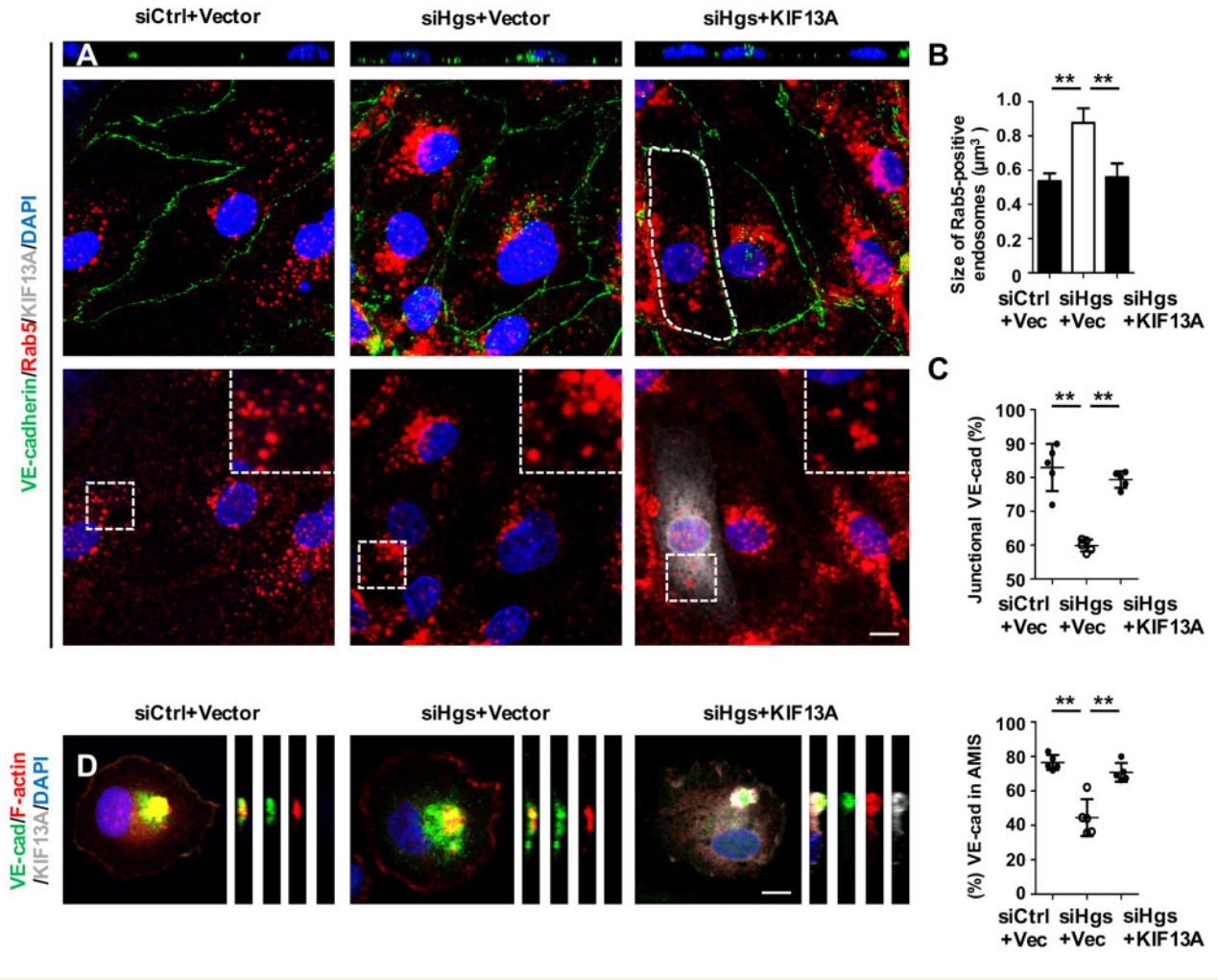


**Figure 7** Restoration of endosomal recycling rescues VE-cadherin polarity in Hgs knockdown ECs. (*A–D*) HUVECs were treated with control or Hgs-siRNA for 24 h and then transfected with control or KIF13A plasmids for 24–48 h before fixation in 4% PFA. (*A*) Confocal images showing that KIF13A overexpression reduced the intracellular accumulation of VE-cadherin and VE-cadherin-containing Rab5-positive early endosomes (upper panel) and normalized the size of Rab5-positive early endosomes (lower panel) in Hgs knockdown HUVECs. Scale bar: 10 μm. (*B*) Quantification of the size of Rab5-positive endosomes (333 endosomes from control HUVECs, 291 endosomes from siHgs-1-treated HUVECs, and 263 endosomes from siHgs-2-treated HUVECs transfected with KIF13A plasmids were analysed). (*C*) Quantification of junctionally distributed VE-cadherin ($n = 5$). (*D*) KIF13A overexpression restored the recruitment of VE-cadherin to the AMIS in Hgs knockdown HUVECs ($n = 5$). Scale bar: 10 μm. Values are presented as means ± standard deviation. $^{**}P < 0.01$ by Mann–Whitney test and one-way analysis of variance.

VE-cadherin to the plasma membrane. The total protein level of VE-cadherin in *Hgs* knockout brain ECs or Hgs-depleted HUVECs was comparable to the controls, indicating that Hgs regulates the endocytic recycling, but not the ESCRT mediated degradation, of VE-cadherin. Previous studies have revealed that the endocytic recycling pathway controls EC barrier integrity through regulating the abundance of VE-cadherin on the membrane. Rab5, a key regulator of early endosomes, is responsible for the LPS-induced internalization of VE-cadherin,[48] and Rab11-positive recycling endosomes mediate VE-cadherin recycling and membrane localization.[49] Our results suggest that ESCRT-regulated endocytic recycling of VE-cadherin controls cerebrovascular EC polarity. We also showed that the kinesin superfamily protein KIF13A is involved in Hgs-regulated endocytic recycling of VE-cadherin, as reinforcing the endosomal recycling by KIF13A overexpression restored the polarized distribution of VE-cadherin at the junctional membrane in Hgs knockdown ECs. Previous studies have revealed that KIF13A cooperates with AP-1 to co-ordinate endosomal sorting and positioning and is required for the morphogenesis of tubular recycling endosomes.[18] Our data suggest that KIF13A plays a critical role in maintaining EC polarity, although the underlying mechanisms need to be further investigated.

Taken together, our study provides the first *in vivo* evidence that Hgs-regulated ESCRT machinery plays an essential role in the maintenance of brain EC polarity and cerebrovascular stability.

## Supplementary material

Supplementary material is available at *Cardiovascular Research* online.

## Authors' contributions

X.Y., Z.Y., and J.Z. conceived and designed this project. Z.Y. and J.Z. performed most of the experiments. Z.Y., J.W., and X.Y. analysed the results. Y.C., X.S., Y.Z., X.Ch., N.H., Y.T., Y.L., and Y.C. contributed materials and comments. X.Y., J.W., and Z.Y. wrote the manuscript.

## Acknowledgements

We thank Naoki Mochizuki (National Cardiovascular Center Research Institute, Osaka, Japan) for the EGFP-VE-cadherin plasmid, and Binbin Han (Institute of Biochemistry and Cell Biology, Chinese Academy Science, Shanghai, China) for technical assistance.

**Conflict of interest:** none declared.

## Funding

This work was supported by the National Natural Science Foundation of China (31430057 and 31630093 to X.Y.), the National Key Research and Development Program of China (2016YFC1300600 to X.Y.), the National Basic Research Program of China (2012CB945103 to X.Y.), and the National Science and Technology Major Projects of Infectious Disease (2017ZX10304402003 to J.W.).

## References

1. Zhao Z, Nelson AR, Betsholtz C, Zlokovic BV. Establishment and dysfunction of the blood-brain barrier. *Cell* 2015;**163**:1064–1078.
2. Worzfeld T, Schwaninger M. Apicobasal polarity of brain endothelial cells. *J Cereb Blood Flow Metab* 2016;**36**:340–362.
3. Lee CY, Bautch VL. Ups and downs of guided vessel sprouting: the role of polarity. *Physiology (Bethesda)* 2011;**26**:326–333.
4. Charpentier MS, Conlon FL. Cellular and molecular mechanisms underlying blood vessel lumen formation. *Bioessays* 2014;**36**:251–259.
5. Strilic B, Kucera T, Eglinger J, Hughes MR, McNagny KM, Tsukita S, Dejana E, Ferrara N, Lammert E. The molecular basis of vascular lumen formation in the developing mouse aorta. *Dev Cell* 2009;**17**:505–515.
6. Lampugnani MG, Orsenigo F, Rudini N, Maddaluno L, Boulday G, Chapon F, Dejana E. CCM1 regulates vascular-lumen organization by inducing endothelial polarity. *J Cell Sci* 2010;**123**:1073–1080.
7. Brinkmann BF, Steinbacher T, Hartmann C, Kummer D, Pajonczyk D, Mirzapourshafiyi F, Nakayama M, Weide T, Gerke V, Ebnet K. VE-cadherin interacts with cell polarity protein Pals1 to regulate vascular lumen formation. *Mol Biol Cell* 2016;**27**:2811–2821.
8. Iden S, Rehder D, August B, Suzuki A, Wolburg-Buchholz K, Wolburg H, Ohno S, Behrens J, Vestweber D, Ebnet K. A distinct PAR complex associates physically with VE-cadherin in vertebrate endothelial cells. *EMBO Rep* 2006;**7**:1239–1246.
9. Gory-Faure S, Prandini MH, Pointu H, Roullot V, Pignot-Paintrand I, Vernet M, Huber P. Role of vascular endothelial-cadherin in vascular morphogenesis. *Development* 1999;**126**:2093–2102.
10. Carmeliet P, Lampugnani MG, Moons L, Breviario F, Compernolle V, Bono F, Balconi G, Spagnuolo R, Oosthuyse B, Dewerchin M, Zanetti A, Angellilo A, Mattot V, Nuyens D, Lutgens E, Clotman F, de Ruiter MC, Gittenberger-de Groot A, Poelmann R, Lupu F, Herbert JM, Collen D, Dejana E. Targeted deficiency or cytosolic truncation of the VE-cadherin gene in mice impairs VEGF-mediated endothelial survival and angiogenesis. *Cell* 1999;**98**:147–157.
11. Montero-Balaguer M, Swirsding K, Orsenigo F, Cotelli F, Mione M, Dejana E. Stable vascular connections and remodeling require full expression of VE-cadherin in zebrafish embryos. *PLoS One* 2009;**4**:e5772.
12. Bentley K, Franco CA, Philippides A, Blanco R, Dierkes M, Gebala V, Stanchi F, Jones M, Aspalter IM, Cagna G, Westrom S, Claesson-Welsh L, Vestweber D, Gerhardt H. The role of differential VE-cadherin dynamics in cell rearrangement during angiogenesis. *Nat Cell Biol* 2014;**16**:309–321.
13. Cao J, Ehling M, Marz S, Seebach J, Tarbashevich K, Sixta T, Pitulescu ME, Werner AC, Flach B, Montanez E, Raz E, Adams RH, Schnittler H. Polarized actin and VE-cadherin dynamics regulate junctional remodelling and cell migration during sprouting angiogenesis. *Nat Commun* 2017;**8**:2210.
14. Eaton S, Martin-Belmonte F. Cargo sorting in the endocytic pathway: a key regulator of cell polarity and tissue dynamics. *Cold Spring Harb Perspect Biol* 2014;**6**:a016899.
15. Cullen PJ, Steinberg F. To degrade or not to degrade: mechanisms and significance of endocytic recycling. *Nat Rev Mol Cell Biol* 2018;**19**:679–696.
16. Grant BD, Donaldson JG. Pathways and mechanisms of endocytic recycling. *Nat Rev Mol Cell Biol* 2009;**10**:597–608.
17. Goldenring JR. Recycling endosomes. *Curr Opin Cell Biol* 2015;**35**:117–122.
18. Delevoye C, Miserey-Lenkei S, Montagnac G, Gilles-Marsens F, Paul-Gilloteaux P, Giordano F, Waharte F, Marks MS, Goud B, Raposo G. Recycling endosome tubule morphogenesis from sorting endosomes requires the kinesin motor KIF13A. *Cell Rep* 2014;**6**:445–454.
19. Rusten TE, Vaccari T, Stenmark H. Shaping development with ESCRTs. *Nat Cell Biol* 2012;**14**:38–45.
20. Henne WM, Buchkovich NJ, Emr SD. The ESCRT pathway. *Dev Cell* 2011;**21**:77–91.
21. Lobert VH, Stenmark H. The ESCRT machinery mediates polarization of fibroblasts through regulation of myosin light chain. *J Cell Sci* 2012;**125**:29–36.
22. Dukes JD, Fish L, Richardson JD, Blaikley E, Burns S, Caunt CJ, Chalmers AD, Whitley P. Functional ESCRT machinery is required for constitutive recycling of claudin-1 and maintenance of polarity in vertebrate epithelial cells. *Mol Biol Cell* 2011;**22**:3192–3205.
23. Frankel EB, Audhya A. ESCRT-dependent cargo sorting at multivesicular endosomes. *Semin Cell Dev Biol* 2018;**74**:4–10.
24. Raiborg C, Stenmark H. The ESCRT machinery in endosomal sorting of ubiquitylated membrane proteins. *Nature* 2009;**458**:445–452.
25. Razi M, Futter CE. Distinct roles for Tsg101 and Hrs in multivesicular body formation and inward vesiculation. *Mol Biol Cell* 2006;**17**:3469–3483.
26. Hanyaloglu AC, McCullagh E, von Zastrow M. Essential role of Hrs in a recycling mechanism mediating functional resensitization of cell signaling. *EMBO J* 2005;**24**:2265–2283.
27. Hasseine LK, Murdaca J, Suavet F, Longnus S, Giorgetti-Peraldi S, Van Obberghen E. Hrs is a positive regulator of VEGF and insulin signaling. *Exp Cell Res* 2007;**313**:1927–1942.
28. Raiborg C, Malerod L, Pedersen NM, Stenmark H. Differential functions of Hrs and ESCRT proteins in endocytic membrane trafficking. *Exp Cell Res* 2008;**314**:801–813.
29. Edgar JR, Willen K, Gouras GK, Futter CE. ESCRTs regulate amyloid precursor protein sorting in multivesicular bodies and intracellular amyloid-beta accumulation. *J Cell Sci* 2015;**128**:2520–2528.
30. Komada M, Soriano P. Hrs, a FYVE finger protein localized to early endosomes, is implicated in vesicular traffic and required for ventral folding morphogenesis. *Genes Dev* 1999;**13**:1475–1485.
31. Watson JA, Bhattacharyya BJ, Vaden JH, Wilson JA, Icyuz M, Howard AD, Phillips E, DeSilva TM, Siegal GP, Bean AJ, King GD, Phillips SE, Miller RJ, Wilson SM. Motor and sensory deficits in the teetering mice result from mutation of the ESCRT component HGS. *PLoS Genet* 2015;**11**:e1005290.
32. Chen J, Hou N, Zhang C, Teng Y, Cheng X, Li Z, Ren J, Zeng J, Li R, Wang W, Yang X, Lan Y. Smooth muscle Hgs deficiency leads to impaired esophageal motility. *Int J Biol Sci* 2015;**11**:794–802.
33. Murakami T, Felinski EA, Antonetti DA. Occludin phosphorylation and ubiquitination regulate tight junction trafficking and vascular endothelial growth factor-induced permeability. *J Biol Chem* 2009;**284**:21036–21046.
34. Meng F, Shi L, Cheng X, Hou N, Wang Y, Teng Y, Meng A, Yang X. Surfactant protein A promoter directs the expression of Cre recombinase in brain microvascular endothelial cells of transgenic mice. *Matrix Biol* 2007;**26**:54–57.
35. Li F, Lan Y, Wang Y, Wang J, Yang G, Meng F, Han H, Meng A, Wang Y, Yang X. Endothelial Smad4 maintains cerebrovascular integrity by activating N-cadherin through cooperation with Notch. *Dev Cell* 2011;**20**:291–302.
36. Li Z, Lan Y, He W, Chen D, Wang J, Zhou F, Wang Y, Sun H, Chen X, Xu C, Li S, Pang Y, Zhang G, Yang L, Zhu L, Fan M, Shang A, Ju Z, Luo L, Ding Y, Guo W, Yuan W, Yang X, Liu B. Mouse embryonic head as a site for hematopoietic stem cell development. *Cell Stem Cell* 2012;**11**:663–675.
37. Baudin B, Bruneel A, Bosselut N, Vaubourdolle M. A protocol for isolation and culture of human umbilical vein endothelial cells. *Nat Protoc* 2007;**2**:481–485.
38. Galvagni F, Baldari CT, Oliviero S, Orlandini M. An apical actin-rich domain drives the establishment of cell polarity during cell adhesion. *Histochem Cell Biol* 2012;**138**:419–433.
39. Giannotta M, Trani M, Dejana E. VE-cadherin and endothelial adherens junctions: active guardians of vascular integrity. *Dev Cell* 2013;**26**:441–454.
40. Brown RC, Morris AP, O'Neil RG. Tight junction protein expression and barrier properties of immortalized mouse brain microvessel endothelial cells. *Brain Res* 2007;**1130**:17–30.
41. Xiao K, Allison DF, Buckley KM, Kottke MD, Vincent PA, Faundez V, Kowalczyk AP. Cellular levels of p120 catenin function as a set point for cadherin expression levels in microvascular endothelial cells. *J Cell Biol* 2003;**163**:535–545.
42. Nakagawa T, Setou M, Seog D, Ogasawara K, Dohmae N, Takio K, Hirokawa N. A novel motor, KIF13A, transports mannose-6-phosphate receptor to plasma membrane through direct interaction with AP-1 complex. *Cell* 2000;**103**:569–581.
43. Moberg KH, Schelble S, Burdick SK, Hariharan IK. Mutations in erupted, the *Drosophila* ortholog of mammalian tumor susceptibility gene 101, elicit non-cell-autonomous overgrowth. *Dev Cell* 2005;**9**:699–710.

44. Vaccari T, Bilder D. The Drosophila tumor suppressor vps25 prevents nonautonomous overproliferation by regulating notch trafficking. *Dev Cell* 2005;**9**:687–698.
45. Fan J, Jiang K, Liu Y, Jia J. Hrs promotes ubiquitination and mediates endosomal trafficking of smoothened in *Drosophila* hedgehog signaling. *PLoS One* 2013;**8**:e79021.
46. Pradhan-Sundd T, Verheyen EM. The Myopic-Ubpy-Hrs nexus enables endosomal recycling of Frizzled. *Mol Biol Cell* 2015;**26**:3329–3342.
47. Leithe E, Kjenseth A, Sirnes S, Stenmark H, Brech A, Rivedal E. Ubiquitylation of the gap junction protein connexin-43 signals its trafficking from early endosomes to lysosomes in a process mediated by Hrs and Tsg101. *J Cell Sci* 2009;**122**:3883–3893.
48. Yang J, Yao W, Qian G, Wei Z, Wu G, Wang G. Rab5-mediated VE-cadherin internalization regulates the barrier function of the lung microvascular endothelium. *Cell Mol Life Sci* 2015;**72**:4849–4866.
49. Yan Z, Wang ZG, Segev N, Hu S, Minshall RD, Dull RO, Zhang M, Malik AB, Hu G. Rab11a mediates vascular endothelial-cadherin recycling and controls endothelial barrier function. *Arterioscler Thromb Vasc Biol* 2016;**36**:339–349.

## Translational perspective

The structural and functional integrity of cerebral vasculature is critical for supporting normal brain function. Mutations of genes that play important roles in blood vessel development cause not only cardiovascular diseases but also neurological disorders. In this study, we discovered a novel physiological function of Hgs in the maintenance of endothelial cell polarity and cerebrovascular stability, demonstrating that endothelial endosomal sorting complex required for transport (ESCRT) machinery has an essential role in maintaining the integrity of cerebral vasculature. This provides insights into the potential pathogenic links between ESCRT dysfunction and cardiovascular diseases, as well as neurodegenerative disorders.